

Theory of Layered Iron Oxide on Frustrated Geometry: Electric Polarization, Magnetoelectric Effect and Orbital State

A. Nagano*, M. Naka, J. Nasu and S. Ishihara

Department of Physics, Tohoku University, Sendai 980-8578, Japan

(Dated: February 8, 2020)

A layered iron oxide $R\text{Fe}_2\text{O}_4$ (R : rare-earth elements) is recognized as a dielectric material with charge-order (CO) driven electric polarization and strong spin-charge coupling. We present a microscopic theory of electronic structure and dielectric property in $R\text{Fe}_2\text{O}_4$. Geometrical frustration in a paired triangle lattice plays a key role for a CO at momentum $\mathbf{q} = (1/3, 1/3)$ accompanied with electric polarization. This polar CO phase is stabilized strongly by a magnetic ordering at $\mathbf{q} = (1/3, 1/3)$. A possibility of an unconventional orbital state in the spin and charge ordered phase is examined.

PACS numbers: 75.80.+q, 77.80.-e, 75.10.-b, 72.80.Ga

Ferroelectric (FE) material has a spontaneous electric polarization induced by displacement of ion and electronic cloud. A subtle balance of long-range Coulomb interaction, lattice potential and electron covalency derives the FE transition and controls the transition temperature. Recently revived magnetoelectric (ME) effects and related multiferroic phenomena [1, 2, 3] are recognized to be spin-driven FE transitions. A key issue is a non-collinear spin structure in frustrated magnets where electric polarization is induced by symmetric and/or antisymmetric exchange strictions. Because of gigantic ME effects observed experimentally, this type of material has been examined from viewpoint of potential application as well as fundamental physics.

Rare-earth iron oxide with layered hexagonal lattice $R\text{Fe}_2\text{O}_4$ (R : rare-earth elements) [4] is a new class of multiferroic material. Paired Fe-O triangle lattices [Fig. 1(a)] and R -O block layers are alternately stacked along the c axis. Since a nominal valence of Fe ion is $2.5+$, an equal amount of Fe^{2+} and Fe^{3+} coexists in the paired triangle lattices. Observations of the Bragg reflections at $(h/3 \ h/3 \ 3m+1/2)$ below $320\text{K} (\equiv T_{\text{CO}}^{3\text{D}})$ in LuFe_2O_4 indicate a valence order of Fe ion, i.e. a three-dimensional (3D) charge order (CO) [5]. Below $250\text{K} (\equiv T_N)$, a ferrimagnetic spin order (SO) has been found by the neutron diffraction experiments where super-structure peaks appear at $(h/3 \ h/3 \ m)$ [6, 7]. It is found that electric polarization appears around $T_{\text{CO}}^{3\text{D}}$ and increases furthermore around T_N [8, 9]. Now, $R\text{Fe}_2\text{O}_4$ is recognized as a multiferroic material with CO driven electric polarization and strong spin-charge coupling.

Being based on the systematic experiments, models for the charge and spin structures have been proposed in Refs. [5, 6, 7]. However, microscopic mechanisms of the FE transition and the multiferroic phenomena have not been clarified. In this Letter, we present a theory of dielectric iron oxides $R\text{Fe}_2\text{O}_4$ with the layered structure. We, in particular, address the following issues: 1) origin of the electric polarization, 2) correlation between electric polarization and magnetic ordering, and 3) orbital degree of freedom in Fe ion. We assert that this material belongs to a new class of systems where novel dielectric properties emerge from interplay among multi-degrees of freedom and geometrical frustration.

Start with electronic state in a single Fe ion. An Fe ion in $R\text{Fe}_2\text{O}_4$ is five-fold coordinate. Three O anions are in the plane and two are at apices. We calculate the crystalline-field splitting for the $3d$ orbitals in a FeO_5 cluster based on the crystal structure data [4]. A point charge of $-2e$ at each O ion and the atomic-like $3d$ orbitals are assumed. Split orbitals are identified by the irreducible representation for the D_{3h} group: the $|d_{3z^2-r^2}\rangle$ (A') orbital, and two sets of the doubly degenerate ones, $\{\cos\theta|d_{yz}\rangle - \sin\theta|d_{xy}\rangle, \cos\theta|d_{zx}\rangle + \sin\theta|d_{x^2-y^2}\rangle\}$ (E'') and $\{\cos\theta|d_{xy}\rangle + \sin\theta|d_{yz}\rangle, \cos\theta|d_{x^2-y^2}\rangle - \sin\theta|d_{zx}\rangle\}$ (E'). It is shown that the degenerate E' orbitals take the lowest energy, and the mixing angle θ is about 0.15π . The energy levels for E' and E'' are close; the energy difference ($\sim 0.2\text{eV}$) between the two is much smaller than that ($\sim 0.8\text{eV}$) between A' and E' . Then, each d orbital is singly occupied in Fe^{3+} ($S = 5/2$), and one of the lowest degenerate orbitals is doubly occupied in Fe^{2+} ($S = 2$). This orbital degree of freedom in Fe^{2+} is treated by the orbital pseudo spin (PS) with an amplitude of $1/2$ [11]: $\mathbf{T}_i = \frac{1}{2} \sum_{\xi, \xi', s} d_{i\xi_s}^\dagger \sigma_{\xi\xi'}^s d_{i\xi'_s}$ where $d_{i\xi_s}$ is the electron annihilation operator with spin s ($=\uparrow, \downarrow$) and orbital ξ ($= d_{x^2-y^2}, d_{xy}$) at site i , and σ are the Pauli matrices. It is convenient to introduce PS for each nearest neighbor (NN) FeO-bond direction in the plane, labeled by $l = (\alpha, \beta, \gamma)$ [see Fig. 1(a)]. We define $\tau_i^l = \cos(2\pi n_l/3) T_i^z + \sin(2\pi n_l/3) T_i^x$ with $(n_\alpha, n_\beta, n_\gamma) = (1, 2, 3)$. The up (down)-eigenstate for τ^l corresponds to the active (inactive) orbital along a direction l .

Now we set up the model Hamiltonian. Even above $T_{\text{CO}}^{3\text{D}}$, the electrical resistivity in $R\text{Fe}_2\text{O}_4$ shows an insulating behavior[12]. This observation indicates that d electrons are almost localized at Fe ions, and incoherent charge motion occurs by thermal electron hopping between Fe^{2+} and Fe^{3+} . We consider that, in such insulating dielectric magnets, the long-range Coulomb repulsion between electronic charges and the superexchange (SE) interaction between spins and orbitals are the dominant interactions. The Coulomb interaction term is given as $\mathcal{H}_V = \sum_{(ij)} V_{ij} n_i n_j$ with the $3d$ -electron number operator $n_i = \sum_{s, \xi} d_{i\xi_s}^\dagger d_{i\xi_s}$ and a pair of Fe sites (ij). This is rewritten as an Ising-like Hamiltonian $\mathcal{H}_V = \sum_{(ij)} V_{ij} Q_i^z Q_j^z$ with the charge conservation $\sum_i Q_i^z = 0$. The PS for charge Q_i^z takes $1/2$ ($-1/2$) for Fe^{2+} (Fe^{3+}). The SE interaction arises

from the virtual electron hopping between in-plane NN Fe ions. For the NN Fe-O-Fe bond with 120° angle, the following two processes are relevant: $d_i^{k_i} d_j^{k_j} \rightarrow d_i^{k_i-1} d_j^{k_j+1} \rightarrow d_i^{k_i} d_j^{k_j}$ (termed U_d process), and $d_i^{k_i} d_j^{k_j} \rightarrow d_i^{k_i+1} \underline{p}^2 d_j^{k_j+1} \rightarrow d_i^{k_i} d_j^{k_j}$ (termed U_p process). A superscript k_i is a number of the d electron at site i , and \underline{p}^2 indicates a two-hole occupied state at the O site. In the strong coupling limit, where the on-site and NN inter-site Coulomb interactions are much larger than the transfer integral t_{pd} between Fe $3d$ and O $2p$, the projection-perturbation theory up to $O(t_{pd}^4)$ is applied [10]. The high-spin 6A_1 (5E) state is chosen as an initial state at Fe^{3+} (Fe^{2+}), and all possible intermediate states, connected with the initial states by t_{pd} , are taken into account. The SE interaction depends on the charge valences in a given pair, $\mathcal{H}_J = \mathcal{H}_{22} + \mathcal{H}_{33} + \mathcal{H}_{23}$, where \mathcal{H}_{nm} is the SE Hamiltonian for NN Fe^{n+} - Fe^{m+} bonds. Each term is divided by the intermediate states \mathcal{I} as $\mathcal{H}_{nm} = \sum_{\mathcal{I}} \mathcal{H}_{nm}^{(\mathcal{I})}$. Here, we show explicitly dominant terms,

$$\begin{aligned} \mathcal{H}_{22}^{(U_d: {}^4T_2 \text{ } {}^6A_1)} &= J_{22}^{(U_d: {}^4T_2 \text{ } {}^6A_1)} \frac{1}{5} \sum_{\langle ij \rangle} \left(\frac{1}{2} \mathbf{I}_i \cdot \mathbf{I}_j + 3 \right) \left(\frac{1}{2} - 2\tau_i^l \tau_j^l \right) \\ &\times \left(\frac{1}{2} - Q_i^z \right) \left(\frac{1}{2} - Q_j^z \right), \end{aligned} \quad (1)$$

$$\begin{aligned} \mathcal{H}_{33}^{(U_d: {}^5E \text{ } {}^5E)} &= J_{33}^{(U_d: {}^5E \text{ } {}^5E)} 4 \sum_{\langle ij \rangle} \left(\frac{1}{25} \mathbf{J}_i \cdot \mathbf{J}_j - \frac{1}{4} \right) \\ &\times \left(\frac{1}{2} + Q_i^z \right) \left(\frac{1}{2} + Q_j^z \right), \end{aligned} \quad (2)$$

$$\begin{aligned} \mathcal{H}_{23}^{(U_d: {}^6A_1 \text{ } {}^5E)} &= J_{23}^{(U_d: {}^6A_1 \text{ } {}^5E)} \frac{2}{5} \sum_{\langle ij \rangle} \left(\frac{1}{5} \mathbf{I}_i \cdot \mathbf{J}_j + \frac{3}{2} \right) \left(\frac{1}{2} - \tau_i^l \right) \\ &\times \left(\frac{1}{2} - Q_j^z \right) \left(\frac{1}{2} + Q_j^z \right), \end{aligned} \quad (3)$$

where \mathbf{I}_i (\mathbf{J}_j) is a spin operator with amplitude 2 ($5/2$), and l in τ_i^l indicates a direction for a given ij bond. $\mathcal{H}_{nm}^{(U_d: \Gamma_1 \Gamma_2)}$ originates from the U_d process with Γ_1 and Γ_2 intermediate states at sites i and j , respectively. The exchange constant $J_{nm}^{(U_d: \Gamma_1 \Gamma_2)} [= -t_{dd}^2 / \Delta E(\Gamma_1 \Gamma_2)]$ is given by the hopping integral t_{dd} between Fe ions and the excitation energy $\Delta E(\Gamma_1 \Gamma_2)$. Details in \mathcal{H}_J will be presented elsewhere. Clearly, spin \mathbf{I}_i (\mathbf{J}_j), charge Q_i^z and orbital τ_i^l degrees of freedom are coupled with each other in \mathcal{H}_J .

First we focus on the charge sector, which is frozen at higher temperature than spin and orbital ordering ones. The Coulomb interaction term \mathcal{H}_V is considered in a pair of the triangle lattices. We introduce, for simplicity, the largest three interactions V_{ij} in a paired layer [see Fig. 1(a)]: the inter-layer NN interaction (V_{cNN}), the intra-layer NN one (V_{abNN}) and the inter-layer next-NN (NNN) one (V_{cNNN}). When the $1/r$ -type Coulomb interaction is assumed, we have $V_{\text{cNN}}/V_{\text{abNN}} = 1.2$ and $V_{\text{cNNN}}/V_{\text{abNN}} = 0.77$ for LuFe_2O_4 . Before going to precise calculations, we have performed the mean-field (MF) calculation to obtain a global phase diagram. In each layer, a periodicity of charge structure is taken up to 12 along [110]

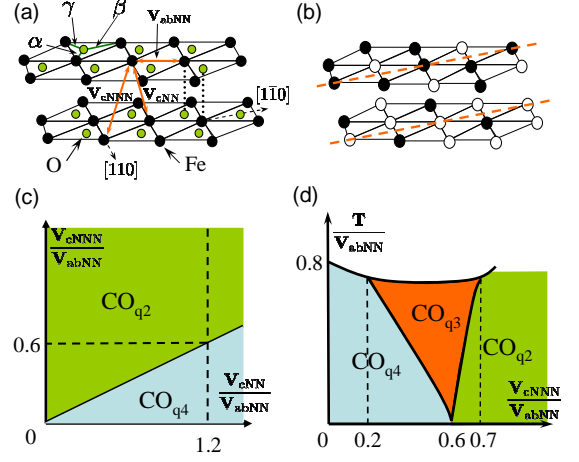


FIG. 1: (a): Fe-O double-layer structure. (b): A schematic view of CO_{q_3} with electric polarization along the c axis. White and black circles represent Fe^{2+} and Fe^{3+} , respectively. (c) and (d) are for the MF phase diagrams at $T = 0$ and finite T calculated in \mathcal{H} , respectively [13]. A value of $V_{\text{cNN}}/V_{\text{abNN}}$ in (d) is chosen to be 1.2.

and [100] directions, and each phase is characterized by the wave number \mathbf{q} in a plane. Let us focus on the three-types of CO: a non-polar CO with $\mathbf{q} = (1/2, 1/2) \equiv \mathbf{q}_2$ (termed CO_{q_2}), that with $(1/4, 1/4) \equiv \mathbf{q}_4$ (CO_{q_4}) and, a polar CO with $(1/3, 1/3) \equiv \mathbf{q}_3$ (CO_{q_3}) [see in Fig. 1(b) and insets of Figs. 2(a) and (c)]. The electric polarization in CO_{q_3} is attributed to the charge imbalance between the two layers [5]; along the [110] direction, a charge alignment is schematically $\dots \bullet \bullet \bullet \bullet \bullet \bullet \bullet \bullet \dots (\dots \circ \circ \circ \circ \circ \circ \circ \circ \dots)$ in the upper (lower) layer, where $\circ (\bullet)$ represents Fe^{2+} (Fe^{3+}). At $T = 0$ [Fig. 1(c)], CO_{q_2} and CO_{q_4} dominate almost whole parameter space, and only on the phase boundary, CO_{q_3} appears together with the two. In finite T [Fig. 1(d)], CO_{q_3} is seen in a wide region between CO_{q_2} and CO_{q_4} [13]. Stability of CO_{q_3} at finite T is caused by an entropy gain due to charge frustration. The Coulomb interactions V_{abNN} at Fe^{3+} (Fe^{2+}) in the upper (lower) layer in Fig. 1(b) are canceled out, and then, charge densities at the sites fluctuate remarkably at finite T .

Unbiased calculations have been performed by utilizing the Monte-Carlo (MC) simulation. A pair of $L \times L$ site cluster ($L = 6, 12$) with the periodic-boundary condition (PBC) is analyzed by the standard MC and multi-canonical MC (MUMC) methods. The energy-density distribution is obtained by the accumulative-recursion method [15] with 20 recursion times, at maximum, and 8×10^6 MC steps are used for measurement based on the energy histogram. The Kawasaki method is used to conserve the total charge density. The T dependence of the charge-correlation function $N(\mathbf{q}) = L^{-2} \sum_{ij} \langle Q_i^z Q_j^z \rangle e^{i\mathbf{q} \cdot (\mathbf{r}_i - \mathbf{r}_j)}$ qualitatively reproduces the global CO phase diagram calculated by the MF method. At $V_{\text{cNNN}}/V_{\text{abNN}} = 0.6$ [Fig. 2(b)], $N(\mathbf{q}_3)$ shows a hump around $T/V_{\text{abNN}} (\equiv T) = 0.18$ and keeps the largest value down to low T . On the other hand, at

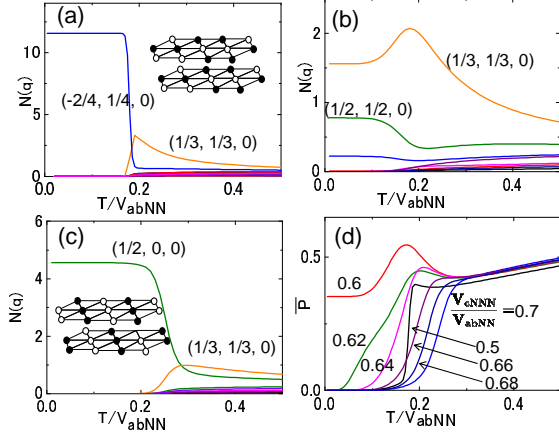


FIG. 2: (a), (b) and (c) are for charge correlation function $N(\mathbf{q})$ at $V_{cNNN}/V_{abNN} = 0.5, 0.6$ and 0.7 , respectively. (d): Electric polarization fluctuation \bar{P} for several V_{cNNN}/V_{abNN} values. A value of V_{cNNN}/V_{abNN} is chosen to be 1.2 . Insets in (a) and (c) represent schematic views of the CO_{q_4} and CO_{q_2} structures, respectively.

$V_{cNNN}/V_{abNN} = 0.5(0.7)$ [Figs. 2(a) and (c)], a main charge correlation function changes from $N(\mathbf{q}_3)$ to $N(\mathbf{q}_2)$ [$N(\mathbf{q}_4)$] with decreasing T . This kind of sequential phase transition from a CO at $(n/3 n/3 0)$ to CO at $(n/2 n/2 0)$ or $(n/4 n/4 0)$ is observed in $\text{YFe}_2\text{O}_{4-\delta}$ [14]. In high temperatures, a dominant charge correlation is seen in $N(\mathbf{q}_3)$ for three cases of V_{cNNN}/V_{abNN} . This may correspond to the observed valence fluctuation along $(h/3 h/3 l)$ above T_{CO}^{3D} [5, 14]. The spontaneous electric polarization is simulated by calculating the polarization fluctuation $\bar{P} = \sqrt{\langle P^2 \rangle}$ [Fig.2(d)]. We define $P = L^{-1}(\sum_{i \in U} - \sum_{i \in L})Q_i^z$ with $\sum_{i \in U(L)}$ being a summation of sites in the upper (lower) layer. At $V_{cNNN}/V_{abNN} = 0.6$, a hump in \bar{P} around $T=0.18$ corresponds to that in $N(\mathbf{q}_3)$. Apart from $V_{cNNN}/V_{abNN} = 0.6$, a reduction of \bar{P} is correlated with the increases of $N(\mathbf{q}_2)$ and $N(\mathbf{q}_4)$. The electric polarization at low T ($\tilde{T} < 0.1$) has been examined more carefully. At $T = 0$, CO_{q_3} degenerates with another type of CO at \mathbf{q}_3 (termed $\overline{\text{CO}}_{q_3}$), which is not taken in the MF calculation. This CO does not show a charge imbalance between the layers, and contains a large number of charge configurations of the order of 2^L . We suppose that, at $T = 0$, \bar{P} vanishes in the thermodynamic limit even at $V_{cNNN}/V_{abNN} = 0.6$. However, since the polar CO_{q_3} degenerates with $\overline{\text{CO}}_{q_3}$, a large dielectric fluctuation is expected to remain at finite T . Actually, we have found in the MUMC calculation performed in two-paired layers that a small value of the inter-double layer Coulomb interaction strongly stabilizes the polar CO_{q_3} .

Now we examine roles of the SE interaction on the electric polarization. The Hamiltonian $\mathcal{H}_V + \mathcal{H}_J$ is analyzed in a pair of the $L \times L$ triangle lattice with $L = 6$ by utilizing the MUMC method. The operator \mathbf{I}_i (\mathbf{J}_i) is assumed to be an Ising spin, and the exchange constants are estimated by using the energy parameters for RFeO_3 [16]. The orbital PSs in \mathcal{H}_J are set to be zero, since we have found by the MC

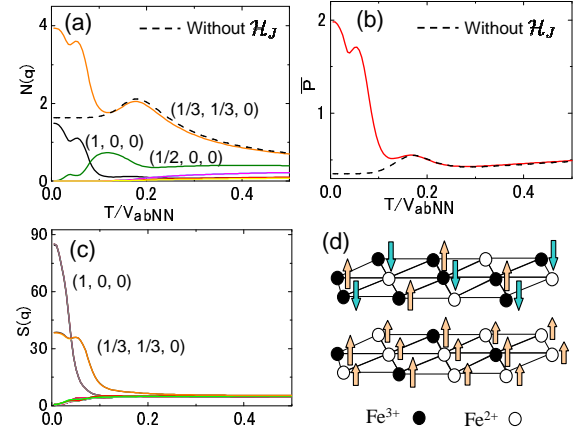


FIG. 3: Charge correlation function $N(\mathbf{q})$ (a), electric polarization fluctuation \bar{P} (b), and spin correlation function $S(\mathbf{q})$ (c) calculated in $\mathcal{H}_V + \mathcal{H}_J$. A schematic view for charge and spin structures is shown in (d). Spin directions at the sites without arrows are not uniquely determined.

calculations that the orbital remains to be disordered much below the CO/SO temperatures. The calculated \bar{P} , $N(\mathbf{q})$ and the spin correlation function $S(\mathbf{q}) = L^{-2} \sum_{ij} \langle S_i^z S_j^z \rangle e^{i\mathbf{q} \cdot (\mathbf{r}_i - \mathbf{r}_j)}$, where S_i^z is I_i^z (J_i^z) for Fe^{2+} (Fe^{3+}), are plotted in Fig. 3. Around $\tilde{T} = 0.18$ in Fig. 3(a), $N(\mathbf{q}_3)$ shows a shoulder, corresponding to a hump in $N(\mathbf{q}_3)$ calculated without \mathcal{H}_J . A further increase in $N(\mathbf{q}_3)$ occurs around $\tilde{T} = 0.1$ ($\equiv T_{\text{SO}}$), being the SO temperature [see Fig. 3(c)]. The T dependence of \bar{P} [Fig. 3(b)] almost follows that of $N(\mathbf{q}_3)$, and reaches its maximum value at $T = 0$. These results clearly show that the SO strongly stabilizes CO_{q_3} with the electric polarization. The spin structure is shown in Fig. 3(d) [17]. This ferrimagnetic structure is consistent with the neutron diffraction experiments [6, 7]. As shown in Fig. 3(d), directions of spins, surrounded by NN three-up and three-down spins, are not determined uniquely. A number of the degenerate spin states is of the order of $2^{L^2/3}$. An entropy gain due to the spin frustration stabilizes this spin structure, and enhances $N(\mathbf{q}_3)$ accompanied with \bar{P} below T_{SO} . The present observation indicates a possibility of large ME response in RFe_2O_4 [18]. By applying magnetic field in the CO/SO phase, melting of CO_{q_3} and reduction of electric polarization are expected.

Finally, we pay our attention to the orbital states. Consider the CO/SO structure shown in Fig.3(d) [19]. It is shown, by applying the relation $\sum_{l=\alpha,\beta,\gamma} \tau_i^l = 0$ to \mathcal{H}_J , that the orbital interactions between NN Fe^{2+} - Fe^{3+} bonds are canceled out. Then, the Hamiltonian \mathcal{H}_J is mapped onto an effective orbital model. This is defined in the Fe^{2+} honeycomb lattice in the 2Fe^{2+} - Fe^{3+} layer [Fig. 4(a)]: $\mathcal{H}_\tau = J \sum_i (\tau_i^\alpha \tau_{i+\delta_{\alpha\beta}}^\beta + \tau_i^\beta \tau_{i+\delta_{\beta\gamma}}^\gamma + \tau_i^\gamma \tau_{i+\delta_{\gamma\alpha}}^\alpha)$ with a NN bond $\delta_{ll'}$, and a coupling constant $J(> 0)$. There is no continuous symmetry in \mathcal{H}_τ . Although the honeycomb lattice is bipartite, a kind of frustration is inherent in \mathcal{H}_τ . When PSs are arranged to gain the energy

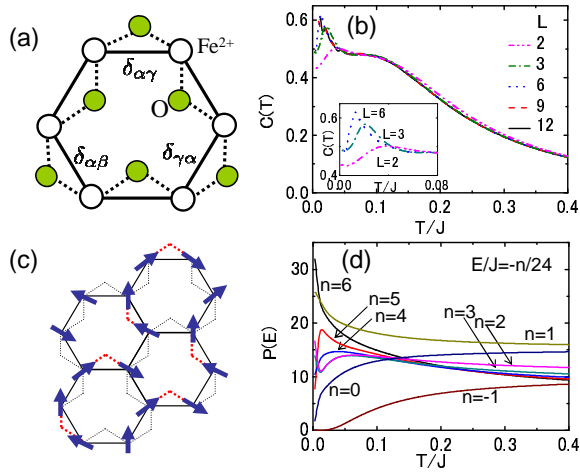


FIG. 4: (a): A schematic picture of the Fe^{2+} -O sublattice in the 2Fe^{2+} - Fe^{3+} layer. (b) Specific heat $C(T)$ for several cluster sizes. Inset shows a magnification for a low T region. (c) One of the GS orbital states. Bold arrows represent the orbital PSs and bold dotted lines indicate Fe-O-Fe bonds where the bond energy is $-J/4$. (d) Bond-energy distribution $P(E)$.

for one NN bond, this is not favorable for other two bonds.

This model provides a non-trivial orbital structure. The Hamiltonian \mathcal{H}_L in a $L \times L$ site cluster ($L = 2 \sim 12$) with PBC is analyzed by using the MUMC method. The orbital PS is treated as a classical vector in the T^x - T^z plane. In the calculated specific heat $C(T)$ [Fig.4(b)], a broad shoulder around $T/J = 0.2$ and a peak at $T_0 (\ll 0.05J)$ appear. The peak shifts to lower T and becomes sharp with increasing L . The orbital correlation functions $\mathcal{F}^{lm}(\mathbf{q}) = L^{-2} \sum_{ij} e^{i\mathbf{q} \cdot (\mathbf{r}_i - \mathbf{r}_j)} \langle T_i^l T_j^m \rangle$ ($l, m = x, z$) for all momenta in a cluster do not show remarkable increase down to low temperatures. Even in the largest $\mathcal{F}^{lm}(\mathbf{q})$ among them, it does not reach 20% of the maximum value. We calculate the number of the NN bonds $P(E)$, which take the bond energy ϵ_B between E and $E + J/24$. Near the lowest temperatures ($\ll T_0$), the obtained $P(E)$ is almost fitted by a function $F(E) = \int_0^{2\pi} d\theta \delta(E + \frac{1}{4}J \cos^2 \theta)$, suggesting rotationally symmetric states at $T = 0$. As shown in Fig. 4(d), a peak is seen at T_0 in $P(-5J/24)$. This implies that the PS configurations with $\epsilon_B \approx -\frac{1}{4}J \cos^2(\pi/6)$ are thermally stabilized. The orbital state at $T = 0$ is examined by using the numerically exact calculation for $L = 2$ where the PS angle is restricted to be $n\pi/6$. We obtain the GS energy per site of $E_\tau^{\text{GS}} = -3J/16$ and the GS orbital structure. One of the GS orbital structures is shown in Fig. 4(c). There is a rule for the PS configuration; in one of the three NN bonds, PSs are aligned to gain the full bond energy of $-J/4$, and in the remaining two bonds, the energy is $-J/16$. In an infinite lattice system, we expect a macroscopic number of the PS configurations which satisfy the rule. Moreover, from one of the GS orbital structures, different degenerate states are created by rotation of all PSs with respect to the T^y axis. This GS state is also suggested

from the analytical way. The orbital Hamiltonian is rewritten as $\mathcal{H}_\tau = \sum_{\langle ij \rangle} (\tilde{\tau}_i^l - \tilde{\tau}_j^l)^2 - (2L^2)3J/16$, which is similar to the so-called e_g -orbital model [20, 21]. Here, PSs on the two sublattices in a hexagonal lattice are rotated by $\pm\pi/6$, and $\tilde{\tau}_i^l$ is defined in the new frame. This form implies that the GS orbital configuration does not depend on the global angle of PSs, and the GS energy per site is $-3J/16$.

Summarizing, a theory of $R\text{Fe}_2\text{O}_4$ is presented. A charge frustration plays a key role for CO_{q_3} accompanied with electric polarization. This CO is strongly stabilized by the ferromagnetic ordering due to the spin frustration and the charge-spin coupling in the SE interaction. The effective orbital model in the CO/SO phase does not show a conventional orbital order, at least, down to $T/J = 0.015$, and a large number of orbital states is degenerate at GS. We assert that $R\text{Fe}_2\text{O}_4$ belongs to a new class of systems where novel dielectric properties emerge from interplay among multi-degrees of freedom and geometrical frustration.

The authors would like to thank N. Ikeda, S. Mori, T. Arima, J. Akimitsu, M. Sasaki, M. Matsumoto, and H. Matsueda for their valuable discussions. This work was supported by JSPS KAKENHI (16340094, 16104005) and TOKUTEI No.451 (18044001) from MEXT, NAREGI, and CREST.

-
- [1] T. Kimura *et al.*, Nature **426**, 55 (2003).
 - [2] K. Saitoh *et al.*, J. Phys. Cond. Mat. **7**, 2855 (1995).
 - [3] N. Hur *et al.*, Nature, **429**, 392 (2004).
 - [4] Kimizuka *et al.*, J. Sol. Stat. Chem. **13**, 176 (1975), and N. Kimizuka *et al.*, in *Handbook on the Physics and Chemistry of Rare Earth* edited by K. A. Gshneider Jr. and L. Eyring, **13**, 283 (Elsevier, 1990).
 - [5] Y. Yamada *et al.*, J. Phys. Soc. Jpn. **66**, 3733 (1997).
 - [6] J. Akimitsu *et al.*, Sol. Stat. Comm. **32**, 1065 (1979).
 - [7] K. Shiratori *et al.*, *Proceedings of the 6th international conference of Ferrites*, 703 (1992).
 - [8] N. Ikeda *et al.*, J. Phys. Soc. Jpn. **69**, 1526 (2000).
 - [9] N. Ikeda *et al.*, Nature **436**, 1136 (2005).
 - [10] A. Nagano, and S. Ishihara, J. Phys. Cond. Mat. (2007).
 - [11] The following discussion for orbital is also applicable to the case where the E'' orbitals are the lowest. In this case, the subscript ξ in $d_{i\xi\sigma}$ takes d_{zx} or d_{yz} , and these orbitals form the π bond with the O $2p_z$ orbital.
 - [12] T. Tanaka *et al.*, Solid Stat. Comm. **44**, 687 (1982).
 - [13] In the MF calculation, where the periodicity of Q_i^z is taken up to 20 sites, we obtain the Devil's flower-type phase diagram. A CO with $\mathbf{q} = (2/7, 2/7)$ in this phase diagram may correspond to the observed CO at $(n/7, n/7)$ in $\text{YFe}_2\text{O}_{4-\delta}$ [14].
 - [14] N. Ikeda *et al.*, Ferroelectrics, **286**, 175 (2003).
 - [15] B. A. Berg, J. Stat. Phys. **82**, 323 (1996).
 - [16] T. Mizokawa, and A. Fujimori, Phys. Rev. B **54**, 5368 (1996).
 - [17] This spin structure is energetically close to the following two structures with $\mathbf{q} = (1/3, 1/3)$: (i) The 2Fe^{3+} - Fe^{2+} layer is the same with that in Fig. 3(d). In the Fe^{3+} - 2Fe^{2+} layer, spins on the Fe^{2+} - Fe^{2+} bonds align antiferromagnetically, and Fe^{3+} spins are not uniquely determined. (ii) The same spin structure proposed in Ref. [7], except that the Fe^{3+} spins in the 2Fe^{3+} - Fe^{2+} layer are not uniquely determined. Stabilities of them are

sensitive to the parameter values. However, the remarkable increases in \bar{P} and $N(\mathbf{q}_3)$ below T_{SO} are commonly observed in the MC calculations for the three parameter sets, where above three spin structures are realized.

[18] A. Subramanian *et al.*, *Adv. Mat.* **18**, 1737 (2006).

[19] The following discussion for derivation of \mathcal{H}_i is also applicable to the two spin structures introduced in Ref. [17].

[20] Z. Nussinov *et al.*, *Euro. Phys. Lett.* **67**, 990 (2004).

[21] A related model is studied in A. Y. Kitaev, *Ann. Phys.* **321**, 2 (2006).

* Present address: Japan Medical Materials Co., Osaka, 532-0003 Japan.